J Biol Phys (2012) 38:209–227
DOI 10.1007/s10867-011-9231-y

ORIGINAL PAPER

The nonlinear chemo-mechanic coupled dynamics of the F_1-ATPase molecular motor

Lizhong Xu · Fang Liu

Received: 21 April 2011 / Accepted: 21 June 2011 /
Published online: 10 August 2011

Abstract The ATP synthase consists of two opposing rotary motors, F_0 and F_1, coupled to each other. When the F_1 motor is not coupled to the F_0 motor, it can work in the direction hydrolyzing ATP, as a nanomotor called F_1-ATPase. It has been reported that the stiffness of the protein varies nonlinearly with increasing load. The nonlinearity has an important effect on the rotating rate of the F_1-ATPase. Here, considering the nonlinearity of the γ shaft stiffness for the F_1-ATPase, a nonlinear chemo-mechanical coupled dynamic model of F_1 motor is proposed. Nonlinear vibration frequencies of the γ shaft and their changes along with the system parameters are investigated. The nonlinear stochastic response of the elastic γ shaft to thermal excitation is analyzed. The results show that the stiffness nonlinearity of the γ shaft causes an increase of the vibration frequency for the F_1 motor, which increases the motor's rotation rate. When the concentration of ATP is relatively high and the load torque is small, the effects of the stiffness nonlinearity on the rotating rates of the F_1 motor are obvious and should be considered. These results are useful for improving calculation of the rotating rate for the F_1 motor and provide insight about the stochastic wave mechanics of F_1-ATPase.

Keywords F_1-ATPase · Molecular motor · Chemo-mechanic coupling · Nonlinearity · Dynamics

1 Introduction

The ATP synthase consists of two opposing rotary motors, F_0 and F_1, coupled to each other. The F_1 motor consists of a hexamer of α and β subunits with stoichiometry $\alpha_3\beta_3$ surrounding a central cavity containing the γ subunit which is a bent coiled-coil. The

L. Xu (✉) · F. Liu
Yanshan University, Qinhuangdao, China 066004
e-mail: xlz@ysu.edu.cn

largest portion of F_0 comprises 12 *c* subunits. These 12 subunits are assembled into a transmembrane disk. The F_1 motor is fueled by nucleotide hydrolysis and drives the γ shaft clockwise (viewed from F_1 toward the membrane), whereas the F_0 motor is fueled by the ion-motive force and drives the γ shaft counterclockwise [1–4]. When the F_1 motor is not coupled to the F_0 motor, it can work in the direction hydrolyzing ATP, as a nanomotor called F_1-ATPase. Rotation of the γ subunit in an isolated F_1 during ATP hydrolysis has been demonstrated experimentally [5–9].

To understand the mechanism of the F_1-ATPase motor, several insightful models have been proposed [10–15]. Yasuda et al. found that the 360° rotation cycle of the γ subunit includes three repeated 120° rotation steps which are further resolved into two substeps of 30° and 90°, and the probability density peaks of finding the γ subunit at some angle correspond to 90°, 120°, 210°, 240°, 330° and 360°. By electrostatic interaction between the β subunits and the coiled coil of the γ subunit, six potential wells are formed between subunits γ and $\alpha_3\beta_3$ [8, 9]. Oster et al. proposed that ATP binding causes elastic strain at the catalytic site and binding of a substrate to the β subunit causes its conformational change (elastic strain) which drives the γ shaft rotation anticlockwise by the electrostatic interactions between γ protrusion and β subunit [16]. The elastic strain potential was considered to be a linear function of the rotational angle of the γ shaft [17]. The characteristic length scales of the F_1-ATPase are about 10 nm and their motion is a stochastic phenomenon which is well observed in the rotation angle of the γ shaft which undergoes small fluctuations due to the random collisions with solvent molecules [8]. The random collisions can induce a random torque. Based on these studies, the authors proposed a stochastic wave mechanics of F_1-ATPase by which a linear chemo-mechanical coupled model for F_1-ATPase was given [18].

However, the mechanics of the protein and DNA has been investigated [19–22]. The force-deformation relationship of the protein is similar to that of DNA. The stiffness of the protein changes along with increasing the force applied to it [20–22]. The nonlinearity has an important effect on the natural frequency of the F_1-ATPase. It will influence the rotating rate of the F_1-ATPase. Therefore, a nonlinear chemo-mechanical coupled dynamic model for F_1-ATPase should be developed.

In this paper, considering the nonlinearity of the γ shaft stiffness for the F_1-ATPase, a nonlinear chemo-mechanical coupled dynamic model of F_1 motor is proposed. Nonlinear vibration frequencies of the γ shaft and their changes along with the system parameters are investigated. The nonlinear stochastic response of the elastic γ shaft to thermal excitation is analyzed. The results show that the stiffness nonlinearity of the γ shaft causes an increase of the vibration frequency for the F_1 motor which increases the motor's rotation rate. When the concentration of ATP is relatively high and the load torque is small, the effects of the stiffness nonlinearity on the rotating rates of the F_1 motor are relatively obvious and should be considered.

2 The chemo-mechanic coupled dynamic equations

Figure 1a shows a view of an electron density map of the F_1–c_{10} complex at 3.9 Å resolution [23]. Figure 1b is the sketch of the F_1 motor. From the figures, it is known that the γ subunit can be considered as an elastic shaft and the γ protrusion at one end of the γ subunit is considered as a lump inertia *J*. The other end of the γ subunit is fixed within the potential well. Setting the origin of the *x* axis at the center of the potential well, *l* is the distance from

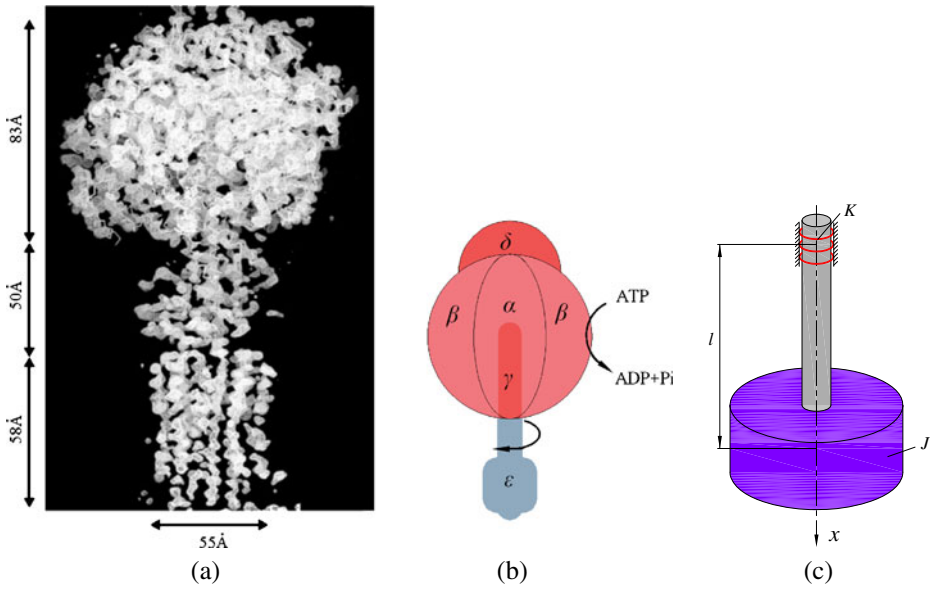

Fig. 1 Electron density map of F_1 and its dynamic model. **a** A view of an electron density map of the F_1–c_{10} complex at 3.9 Å resolution. **b** Sketch of the F_1 motor **c** Dynamic wave model of the γ subunit. Figure 1a is reprinted from [23], with permission from AAAS

the origin to the center of the structure with lump inertia J. Thus, the dynamic wave model of the γ subunit can be given as shown in Fig. 1c (here, k is stiffness of the potential well).

The stochastic twisting wave of the elastic γ shaft can be described by its dynamic equation

$$\tau_f + \tau_e + \tau_i + \tau_{\text{fluct}} = 0 \tag{1}$$

with the dynamic viscous torque $\tau_f = -\frac{d\theta(x,t)}{dt}\zeta$ (here, $\theta(x,t)$ is the dynamic twisting angle displacement of the γ shaft, x is the coordinate of one point on the γ shaft, t is time, ζ is the drag coefficient between the γ shaft and water); dynamic elastic torque $\tau_e = GI_p\frac{\partial^2\theta(x,t)}{\partial x^2}$ (here, G is the shear modulus of elasticity, I_p is the rotary inertia of the γ shaft); inertia torque $\tau_i = -\rho I_p\frac{\partial^2\theta(x,t)}{\partial t^2}$ (here, ρ is density of the protein); τ_{fluct} is the Brownian torque from thermal fluctuations. It is taken as a Gaussian white noise related to drag coefficient ζ_2 according to the fluctuation–dissipation theorem

$$\langle \tau_{\text{fluct}}(t) \rangle = 0 \tag{2}$$

$$\left\langle \tau_{\text{fluct}}(t)\, \tau_{\text{fluct}}\left(t'\right)\right\rangle = 2k_B T\zeta_2\delta\left(t-t'\right) \tag{3}$$

where ζ_2 is the friction coefficient between the γ protrusion and water, k_B is the Boltzmann constant, and T is the temperature.

Substituting the related torques into 1, the stochastic dynamic equation of the elastic γ shaft can be given as

$$\rho I_p\frac{\partial^2\theta(x,t)}{\partial t^2} + \zeta\frac{\partial\theta(x,t)}{\partial t} - GI_p\frac{\partial^2\theta(x,t)}{\partial x^2} = \tau_{\text{fluct}}. \tag{4}$$

The shear modulus of elasticity G of the γ shaft is nonlinear and can be expressed as

$$G = G_0 + b\theta_T + \frac{b^2}{G_0}\theta_T^2 + \cdots = G_0\left(1 + \frac{b^2}{G_0}\theta_T + \frac{b^2}{G_0^2}\theta_T^2 + \cdots\right) \tag{5}$$

where G_0 is the linear shear modulus of elasticity of the γ shaft, b is a coefficient, θ_T is the twisting angle displacement of the γ shaft, $\theta_T = \theta_0 + \theta$, θ_0 is the static twisting angle displacement of the γ shaft.

The static twisting angle displacement θ_0 can be calculated by

$$\theta_0 = \frac{\tau_s}{GI_p} \tag{6}$$

where τ_s is the static torque applied to the γ subunit, $\tau_s = \tau_{\text{drive}} - \tau_{\text{load}}$, τ_{drive} is the driving torque applied to the γ the subunit, which equals the derivative of the membrane potential with respect to the γ subunit position angle, $\tau_{\text{drive}} = 3\Delta\mu_e/2\pi$ (here, $\Delta\mu_e$ is the work done in hydrolyzing one ATP). It is a chemo-mechanic coupled term which represents the influence of the chemical energy on mechanical motion. τ_{load} is load torque applied to the γ the subunit (trans-membrane ion gradient, torque from laser trap, or torque from electromagnet).

Set small parameter $\varepsilon = \frac{b}{G_0}$, and then Eq. 5 can be changed into

$$G = G_0\left(1 + \varepsilon\theta_T + \varepsilon^2\theta_T^2 + \cdots\right). \tag{7}$$

Substituting Eq. 7 into Eq. 4 yields

$$\rho I_p\frac{\partial^2\theta(x,t)}{\partial t^2} + \zeta\frac{\partial\theta(x,t)}{\partial t} - G_0\left(1 + \varepsilon\theta_T + \varepsilon^2\theta_T^2 + \cdots\right)I_p\frac{\partial^2\theta(x,t)}{\partial x^2} = \tau_{\text{fluct}}. \tag{8}$$

Neglecting high-order terms, we find

$$\frac{\partial^2\theta(x,t)}{\partial t^2} + \xi_1\frac{\partial\theta(x,t)}{\partial t} - \frac{G_0\left(1 + \varepsilon\theta_T + \varepsilon^2\theta_T^2\right)}{\rho}\frac{\partial^2\theta(x,t)}{\partial x^2} = \tau_{\text{fluct}e} \tag{9}$$

where $\xi_1 = \zeta/\rho I_p$ and $\tau_{\text{fluct}e} = \tau_{\text{fluct}}/\rho I_p$.

Substituting $\theta_T = \theta_0 + \theta$ into Eq. 9, yields

$$\frac{\partial^2\theta(x,t)}{\partial t^2} + \zeta_1\frac{\partial\theta(x,t)}{\partial t} - G_0\left(1 + \varepsilon(\theta_0 + \theta) + \varepsilon^2(\theta_0 + \theta)^2\right)\frac{I_p}{\rho}\frac{\partial^2\theta(x,t)}{\partial x^2} = \tau_{\text{fluct}e}. \tag{10}$$

Equation 10 is just the chemo-mechanic coupled dynamic equation. θ_0 is the chemo-mechanic coupled term dependent on the chemical potential across the membrane, which represents the effects of the chemical energy on mechanical motion.

3 The solution of the chemo-mechanic coupled dynamic equation

Neglecting the damping term and the exciting torque, substituting $\theta(x,t) = \phi(x)q(t)$ into Eq. 10, yields

$$\frac{G_0}{\rho}\frac{\ddot{\phi}(x)}{\phi(x)} = \frac{1}{\left[1 + \varepsilon\left(\theta_0 + \bar{\phi}q(t)\right) + \varepsilon^2\left(\theta_0^2 + 2\theta_0\bar{\phi}q(t) + \bar{\phi}^2q(t)^2\right)\right]}\frac{\ddot{q}(t)}{q(t)} \tag{11}$$

where $\bar{\phi} \approx \frac{1}{l}\int_0^l\sum\phi_i(x)$ and $\bar{\phi}^2 = \frac{1}{l}\int_0^l\sum\phi_i^2(x)$, $\phi(x)$ is the mode function of the γ shaft.

Let Eq. 11 equal constant $-\omega_0^2$, thus

$$\phi''(x) + \left(\frac{\omega_0}{a}\right)^2 \phi(x) = 0, \tag{12}$$

$$\ddot{q}(t) + \omega_0^2 \left[1 + \varepsilon\left(\theta_0 + \bar{\phi} q(t)\right) + \varepsilon^2 G_0 \left(\theta_0^2 + 2\theta_0 \bar{\phi} q(t) + \bar{\phi}^2 q^2(t)\right)\right] q(t) = 0 \tag{13}$$

where $a = \sqrt{G_0/\rho}$.

The solution of Eq. 12 can be written as

$$\phi(x) = C_1 \sin\frac{\omega}{a}x + C_2 \cos\frac{\omega}{a}x. \tag{14}$$

Thus, the boundary conditions of the γ subunit can be given by $GI_p\phi'(0) = k\phi(0)$ and $GI_p\phi'(l) = J\omega^2\phi(l)$. Substituting Eq. 14 into the boundary conditions yields

$$tg\frac{\omega}{a}l = GI_p\frac{\omega}{a}\frac{k - J\omega^2}{\left(GI\frac{\omega}{a}\right)^2 + kJ\omega^2}. \tag{15}$$

From Eq. 15, the natural frequency of the linear vibration for the γ subunit can be obtained. Substituting the natural frequency into 14, the mode function can be given as

$$\phi_i(x) = \frac{k}{GI_p}\frac{a}{\omega_i}\sin\frac{\omega_i}{a}x + \cos\frac{\omega_i}{a}x \quad (i = 1, 2, \ldots, n) \tag{16}$$

where ω_i is the ith-order natural frequency of the γ subunit, and $\phi_i(x)$ is the ith-order mode function.

Using the Lindstedt-Poincaré method, one assumes

$$q(t, \varepsilon) = q_0(t) + \varepsilon q_1(t) + \varepsilon^2 q_2(t) + \ldots\ldots \tag{17}$$

and

$$\omega^2 = \omega_0^2\left(1 + \varepsilon\sigma_1 + \varepsilon^2\sigma_2 + \ldots\ldots\right) \tag{18}$$

where ω is the nonlinear vibration frequency.

Substituting Eqs. 17 and 18 into 13, and equating coefficients of like powers of ε on both sides, one obtains

$$\ddot{q}_0 + \omega^2 q_0 = 0, \tag{19a}$$

$$\ddot{q}_1 + \omega^2 q_1 = -\omega^2\left(\sigma_1 q_0 + \theta_0 q_0 + \bar{\phi} q_0^2\right), \tag{19b}$$

$$\begin{aligned}\ddot{q}_2 + \omega^2 q_2 = -\omega^2 \big(&\theta_0 q_1 + 2\bar{\phi} q_0 q_1 + 2G_0\bar{\phi}\theta_0 q_0^2 + G_0\theta_0^2 q_0 - \theta_0^2 q_0 \\ &- \theta_0\bar{\phi} q_0^2 + \sigma_2 q_0 + \sigma_1 q_1 + G_0\bar{\phi}^2 q_0^3\big).\end{aligned} \tag{19c}$$

Here, the initial conditions are

$$\left.\begin{array}{l} q_0(0) = Q_0, \dot{q}_0(0) = 0 \\ q_1(0) = 0, \dot{q}_1(0) = 0 \\ q_2(0) = 0, \dot{q}_2(0) = 0 \\ \ldots\ldots \end{array}\right\} \tag{20}$$

The solution of Eq. 19a under the above initial conditions is

$$q_0 = Q_0 \cos \omega t \tag{21}$$

Substituting Eq. 21 into Eq. 19b yields

$$\ddot{q}_1 + \omega^2 q_1 = -\omega^2 \left[(\sigma_1 + \theta_0)\, Q_0 \cos \omega t + \frac{1}{2} \bar{\phi} Q_0^2 \left(1 + \cos 2\omega t\right) \right] \tag{22}$$

In order to remove the secular term, i.e., that which grows without bound, let the coefficient of cos ωt be zero, and then

$$\sigma_1 = -\theta_0. \tag{23}$$

Thus

$$q_1 (t) = -\frac{Q_0^2 \bar{\phi}}{2} + \frac{Q_0^2 \bar{\phi}}{3} \cos \omega t + \frac{Q_0^2 \bar{\phi}}{6} \cos 2\omega t. \tag{24}$$

Substituting Eqs. 21 and 24 into (19c) yields

$$\begin{aligned} \ddot{q}_2 + \omega^2 q_2 = \; & -\omega^2 \left[\left(G_0 \theta_0^2 - \theta_0^2 - \sigma_2 - Q_0^2 \left(\bar{\phi}\right)^2 + G_0 Q_0^2 \bar{\phi}^2 + \frac{1}{6} Q_0^2 \left(\bar{\phi}\right)^2 \right) \right. \\ & \left. \times\, Q_0 \cos \omega t + b_1 \left(1 + \cos 2\omega t\right) + b_2 \cos 3\omega t \right] \end{aligned} \tag{25}$$

where $b_1 = \frac{1}{3} Q_0^3 \bar{\phi}^2 + G_0 Q_0^2 \theta_0 \bar{\phi} - \frac{1}{2} Q_0^2 \theta_0 \bar{\phi}$ and $b_2 = \frac{1}{6} Q_0^3 \left(\bar{\phi}\right)^2 + \frac{1}{2} G_0 Q_0^3 \bar{\phi}^2$.

In order to remove the secular term, let coefficient of the cos ωt to be zero, and then

$$\sigma_2 = G_0 \theta_0^2 - \theta_0^2 - \frac{5}{6} Q_0^2 \left(\bar{\phi}\right)^2 + G_0 Q_0^2 \bar{\phi}^2. \tag{26}$$

Thus

$$q_2 (t) = -b_1 + \left(\frac{2}{3} b_1 - \frac{1}{8} b_2 \right) \cos \omega t + \frac{1}{3} b_1 \cos 2\omega t + \frac{1}{8} b_2 \cos 3\omega t. \tag{27}$$

Substituting Eqs. 21, 24, and 27 into (17) yields

$$\begin{aligned} q (t) = \; & Q_0 \cos \omega t - \varepsilon \frac{Q_0^2 \bar{\phi}}{6} \left(3 - 2 \cos \omega t - \cos 2\omega t\right) \\ & - \varepsilon^2 \left(-b_1 + \left(\frac{2}{3} b_1 - \frac{1}{8} b_2 \right) \cos \omega t + \frac{1}{3} b_1 \cos 2\omega t + \frac{1}{8} b_2 \cos 3\omega t \right). \end{aligned} \tag{28}$$

Substituting Eq. 14 and 28 into $\theta (x, t) = \phi (x)\, q (t)$, the nonlinear free vibration displacements of the γ shaft can be obtained. Substituting Eqs. 23 and 26 into (18), the nonlinear vibration frequency of the γ shaft can also be given as

$$\omega^2 = \omega_0^2 \left[1 - \varepsilon \theta_0 + \varepsilon^2 \left(G_0 \theta_0^2 - \theta_0^2 - \frac{5}{6} Q_0^2 \left(\bar{\phi}\right)^2 + G_0 Q_0^2 \bar{\phi}^2 \right) \right]. \tag{29}$$

4 Stochastic response of the elastic γ shaft to thermal excitation

4.1 Linear stochastic response

After mode functions are obtained, the stochastic response of the elastic γ shaft to thermal excitation can be resolved. The solution of Eq. 10 can be given in the following form:

$$\theta(x,t) = \sum_{i=1}^{\infty} \phi_i(x)\, q_i(x). \tag{30}$$

Substituting Eq. 30 into (10), letting $\varepsilon = 0$, and using the orthogonality of the mode function, yields

$$\ddot{q}_i(t) + 2\xi_i\omega_i\dot{q}_i(t) + \omega_i^2 q_i(t) = Q_i(t) \quad (i = 1, 2, \ldots, n) \tag{31}$$

where $q_i(t)$ is the generalized coordinate of the γ subunit wave, $Q_i(t)$ is the generalized force, and ξ_i is the relative damping coefficient.

The generalized force is

$$Q_i(t) = \int_0^l \varphi_i(x)\, \tau_{\text{fluct}}(x,t)\, dx. \tag{32}$$

As the thermal excitation applied to the γ protrusion has the most important influence on the stochastic wave of the γ subunit, the fluctuating torque can be written as

$$\tau_{\text{fluct}}(x,t) = \tau_{\text{fluct}}(t)\,\delta(x-l). \tag{33}$$

Substituting Eq. 33 into (32) yields

$$Q_i(t) = \varphi_i(l)\,\tau_{\text{fluct}}(t). \tag{34}$$

Thus, the RMS value of the γ subunit wave at any point x_p can be given as

$$E\left[\theta^2(x_p,t)\right] = \frac{1}{2\pi}\sum_{j=1}^{\infty} 2k_BT\zeta_2\phi_j^2(x_p)\phi_j^2(l)\int_{-\infty}^{+\infty}\left|H_j(\omega)\right|^2 d\omega \tag{35}$$

where $H_i(\omega)$ is the complex frequency response function between the thermal excitation and the twisting wave of the γ subunit.

From Eq. 10, the complex frequency response function can be deduced:

$$H_j(\omega) = \frac{1}{\omega_j^2 - \omega^2 + 2i\omega\omega_j}. \tag{36}$$

Substituting Eq. 36 into (35) yields

$$E\left[\theta^2(x_p,t)\right] = \frac{k_BT\zeta_2}{2}\sum_{j=1}^{\infty}\phi_j^2(x_p)\phi_j^2(l)\frac{1}{\xi_j\omega_j^3}. \tag{37}$$

The rotating rate of the γ subunit is mainly decided by the wave of the partial subunit within the potential well. As one end of the potential well, $x = 0$. Hence, the RMS value of the γ subunit wave at point $x = 0$ is

$$E\left[\theta^2(0,t)\right] = \frac{k_BT\zeta_2}{2}\sum_{j=1}^{\infty}\phi_j^2(0)\phi_j^2(l)\frac{1}{\xi_j\omega_j^3}. \tag{38}$$

In Eq. 38, the wave amplitude of the lowest mode of the γ subunit is the maximum. The lowest mode wave plays the main role for escape of the γ subunit from the potential well.

Let σ_θ denote the root mean square error of the wave for the γ subunit at its one end (within potential well, $x = 0$). Then, the root mean square error can be calculated from Eq. 38 easily.

4.2 Nonlinear stochastic response

Based on the linear stochastic response of the elastic γ shaft to thermal excitation, the nonlinear stochastic response can be obtained as well. Substituting Eq. 30 into (10), using the orthogonality of the mode function yields

$$\ddot{q}_i(t) + 2\xi_i\omega_i\dot{q}_i(t) + \omega_i^2 q_i(t) + \omega_i^2\left[\varepsilon\left(\theta_0 + \bar{\phi}q_i(t)\right) + \varepsilon^2\left(\theta_0 + \bar{\phi}q_i(t)\right)^2\right]q_i(t) = Q_i(t)$$
$$(i = 1, 2, \ldots, n). \tag{39}$$

Let $g(q_i(t))$ denote the nonlinear term of Eq. 39, thus

$$g(q_i(t)) = \omega_i^2\left[\varepsilon\left(\theta_0 + \bar{\phi}q_i(t)\right) + \varepsilon^2\left(\theta_0 + \bar{\phi}q_i(t)\right)^2\right]q_i(t). \tag{40}$$

The equivalent linear equation for Eq. 39 can be given in the following form

$$\ddot{q}_i(t) + 2\xi_{ie}\omega_i\dot{q}_i(t) + k_{ie}q_i(t) = Q_i(t) \tag{41}$$

where ξ_e and k_e are the equivalent damping and stiffness coefficients, respectively.

The difference between Eq. 39 and 41 is

$$e(q_i(t), \dot{q}_i(t)) = 2\omega_i(\xi_i - \xi_{ie})\dot{q}_i(t) + \left(\omega_i^2 - k_{ie}\right)q_i(t) + g(q_i(t)). \tag{42}$$

In order to determine coefficients ξ_e and k_e, the following conditions should be met:

$$\frac{\partial E\left(e^2\right)}{\partial \xi_e} = 0 \tag{43a}$$

and

$$\frac{\partial E\left(e^2\right)}{\partial k_e} = 0, \tag{43b}$$

where $E(e^2)$ is the variance of the function $e(q_i(t), \dot{q}_i(t))$.

Substituting Eq. 42 into (43a) and (43b) yields

$$\left.\begin{aligned} 2\omega_i(\xi_i - \xi_{ie})E\left[\dot{q}_i^2(t)\right] + \left(\omega_i^2 - k_e\right)E[q_i(t)\dot{q}_i(t)] + E[\dot{q}_i(t)g(q_i(t))] = 0 \\ 2\omega_i(\xi_i - \xi_{ie})E[q_i(t)\dot{q}_2(t)] + \left(\omega_0^2 - k_e\right)E\left[q_i^2(t)\right] + E[q_i(t)g(q_i(t))] = 0 \end{aligned}\right\} \tag{44}$$

From Eq. 44, the coefficients ξ_e and k_e can be obtained:

$$\left.\begin{aligned} \xi_{ie} &= \xi_i + \frac{E\left[q_i^2(t)\right]E[\dot{q}_i(t)g(q_i(t))] - E[q_i(t)\dot{q}_i(t)]E[q_i(t)g(q_i(t))]}{2\omega_i E\left[\dot{q}_i^2(t)\right]E\left[q_i^2(t)\right] - (E[q_i(t)\dot{q}_i(t)])^2} \\ k_e &= \omega_i^2 + \frac{E\left[\dot{q}_i^2(t)\right]E[q_i(t)g(q_i(t))] - E[q_i(t)\dot{q}_i(t)]E[\dot{q}_i(t)g(q_i(t))]}{E\left[\dot{q}_i^2(t)\right]E\left[q_i^2(t)\right] - (E[q_i(t)\dot{q}_i(t)])^2} \end{aligned}\right\} \tag{45}$$

The thermal fluctuations are considered as steady Gaussian white noise, thus

$$E[q_i(t)\dot{q}_i(t)] = 0. \tag{46}$$

Thus, Eq. 45 can be changed into the following form:

$$\left.\begin{aligned} \xi_{ie} &= \xi_i \\ k_e &= \omega_i^2 + \frac{E\left[q_i\left(t\right) g\left(q_i\left(t\right)\right)\right]}{E\left[q_i^2\left(t\right)\right]} \end{aligned}\right\} \tag{47}$$

For the steady Gaussian white noise, $E\left[q_i^2\left(t\right)\right]$ can be given by

$$E\left[q_i^2\left(t\right)\right] = \frac{S_0}{2\xi_e k_e} = E\left[q_{i0}^2\left(t\right)\right]\frac{\omega_i^2}{k_e} \tag{48}$$

where $E\left[q_{i0}^2\left(t\right)\right] = S_0/\left(2\xi_i\omega_i^2\right)$, and gives the variance of the linear system.

Substituting Eq. 40 into (47) yields

$$k_e = \omega_i^2\left[1 + \varepsilon\theta_0 + \varepsilon^2\theta_0^2 + \frac{2\sqrt{2}}{\sqrt{\pi}}\varepsilon\bar{\phi}\left(1 + 2\varepsilon\theta_0\right)\left(\frac{\sigma_\theta}{\phi_i\left(0\right)}\right)^3 + 3\varepsilon^2\bar{\phi}^2 E\left[q_i^2\left(t\right)\right]\right. . \tag{49}$$

Combining Eq. 48 with 49 yields

$$\begin{aligned} &3\varepsilon^2\bar{\phi}^2\left(E\left[q_i^2\left(t\right)\right]\right)^2 + \left(1 + \varepsilon\theta_0 + \varepsilon^2\theta_0^2\right)E\left[q_i^2\left(t\right)\right] \\ &\quad + \frac{2\sqrt{2}}{\sqrt{\pi}}\varepsilon\bar{\phi}\left(1 + 2\varepsilon\theta_0\right)\left(\frac{\sigma_\theta}{\phi_i\left(0\right)}\right)^3 - E\left[q_{i0}^2\left(t\right)\right]\Big] = 0. \end{aligned} \tag{50}$$

Each term of Eq. 50 is multiplied by $\phi_i^2\left(x_p\right)$, giving

$$\begin{aligned} &\frac{3\varepsilon^2\bar{\varphi}^2}{\varphi_i^2\left(x_p\right)}\left(E\left[\theta_{\text{non}}^2\left(x_p, t\right)\right]\right)^2 + \left(1 + \varepsilon\theta_0 + \varepsilon^2\theta_0^2\right)E\left[\theta_{\text{non}}^2\left(x_p, t\right)\right] \\ &\quad + \frac{2\sqrt{2}}{\sqrt{\pi}}\varepsilon\bar{\varphi}\left(1 + 2\varepsilon\theta_0\right)\left(\frac{\sigma_\theta}{\varphi_i\left(0\right)}\right)^3\varphi_i^2\left(x_p\right) - E\left[\theta^2\left(x_p, t\right)\right] = 0 \end{aligned} \tag{51}$$

where $E\left[\theta^2\left(x_p, t\right)\right]$ and $E\left[\theta_{\text{non}}^2\left(x_p, t\right)\right]$ are the wave variance of the dynamic angle at point x_p for linear and nonlinear systems, respectively.

From Eq. 51, one obtains

$$E\left[\theta_{\text{non}}^2\left(x_p, t\right)\right] = \frac{\varphi_i^2\left(x_p\right)}{6\varepsilon^2\bar{\varphi}^2}\left(-1 - \varepsilon\theta_0 - \varepsilon^2\theta_0^2 + \sqrt{\Delta}\right) \tag{52}$$

where $\Delta = 1 + 2\varepsilon\theta_0 + 3\varepsilon^2\theta_0^2 + 12\varepsilon^2\bar{\phi}^2 E\left[\theta^2\left(x_p, t\right)\right]$.

Equation 52 can be written as

$$\begin{aligned} E\left[\theta_{\text{non}}^2\left(x_p, t\right)\right] = \ &\varphi_i^2\left(x_p\right)\left[-\frac{1}{48\varepsilon^2\bar{\varphi}^2} - \frac{\theta_0}{12\varepsilon\bar{\varphi}^2} - \frac{\theta_0^2}{8\bar{\varphi}^2} + \left(\frac{1}{2} - \varepsilon\theta_0 - \frac{3}{2}\varepsilon^2\theta_0^2\right)\right. \\ &\left.\times E\left[\theta^2\left(x_p, t\right)\right] - 3\varepsilon^2\bar{\varphi}^2\left(E\left[\theta^2\left(x_p, t\right)\right]\right)^2\right]. \end{aligned} \tag{53}$$

The wave variance of the dynamic angle at point $x_p = 0$ can be given as

$$\begin{aligned} E\left[\theta_{\text{non}}^2\left(0, t\right)\right] = \ &\varphi_i^2\left(0\right)\left[-\frac{1}{48\varepsilon^2\bar{\varphi}^2} - \frac{\theta_0}{12\varepsilon\bar{\varphi}^2} - \frac{\theta_0^2}{8\bar{\varphi}^2} + \left(\frac{1}{2} - \varepsilon\theta_0 - \frac{3}{2}\varepsilon^2\theta_0^2\right)\right. \\ &\left.\times E\left[\theta^2\left(0, t\right)\right] - 3\varepsilon^2\bar{\varphi}^2\left(E\left[\theta^2\left(0, t\right)\right]\right)^2\right] \end{aligned} \tag{54}$$

5 The rotation rate of the γ subunit

The rotation rate of the γ subunit can be given as

$$f = \frac{1}{3t_{1/3}} \tag{55}$$

where $t_{1/3}$ denote a 120° rotation time of the γ subunit, $t_{1/3} = t_{\text{mech}} + t_{\text{reac}} + t_{\text{coup}}$. t_{mech} is the time of the γ subunit for 120° mechanical step, $t_{\text{mech}} = \frac{1}{k_h} + \frac{1}{k'_h}$, consisting of 90° and 30° mechanical substep times; here, $t_{\text{mech90}^0} = \frac{1}{k_h}$ and $t_{\text{mech30}^0} = \frac{1}{k'_h}$. t_{reac} is the reaction time of the ATPase, $t_{\text{reac}} = \frac{1}{k_T[T]} + \frac{1}{k_{-D}} + \frac{1}{k_{-P}} + \frac{1}{k_{-P}}\frac{k_D[D]}{k_{-D}}$. t_{coup} is the coupled time of the γ subunit rotation and ADP, P_i dissociation, $t_{\text{coup}} = \frac{1}{k'_h}\frac{k_P[P]}{k_{-P}}\left(1 + \frac{k_D[D]}{k_{-D}}\right)$. $[T]$, $[D]$, and $[P]$ are the concentration of ATP, ADP, and P_i, respectively; k_h is the rate of 90° rotation of the γ subunit of the F_1-ATPase, k'_h is its rate of 30° rotation; k_x is the binding rate constant for species x, k_{-x} is the corresponding dissociation rate constant ($x = T$, D, or P).

The static balance equation of the γ shaft rotation can be described by

$$\tau_{\text{drive}} - \tau_{\text{load}} - k\theta_{\text{end}} = 0 \quad \text{(within potential well)} \tag{56a}$$

$$\tau_{\text{drive}} - \tau_{\text{load}} - \frac{d\phi}{dt}\zeta = 0 \quad \text{(outside potential well)} \tag{56b}$$

where k is the stiffness of the potential well, and θ_{end} is the shift amount of the partial γ subunit within the potential well. ϕ is the rotation angle of the γ subunit, and ζ is the friction coefficient between the actin filament or the bead and the water.

From Eq. 56a, the shift amount θ_{end} of the partial γ subunit within the potential well can be given. Thus, the probability density function $p(\theta)$ of the γ subunit wave can be determined $\left(p(\theta) = \frac{1}{\sqrt{2\pi}\sigma_\theta} e^{-\frac{(\theta-\theta_{\text{end}})^2}{2\sigma_\theta^2}}\right)$ and the probability P_α of the γ subunit escape from the potential well can be calculated ($P_\alpha = \int_{\alpha/2}^{\infty} p(\theta)\, d\theta - \int_{-\infty}^{-\alpha/2} p(\theta)\, d\theta$, where α is the width of the potential well). So, the oscillation time t_α of the γ subunit within the potential well before escape is

$$t_\alpha = 2\pi \big/ (P_\alpha \omega_1), \tag{57}$$

where ω_1 is the lowest vibration frequency of the γ subunit.

Let β denote the angular distance between the two potential wells. Then, from Eq. 56b, the jumping time from one well to another can be obtained:

$$t_\beta = \frac{\beta\xi}{\tau_{\text{drive}} - \tau_{\text{load}}}. \tag{58}$$

As state above, a 120° rotation has been resolved into two substeps of approximately 30° and 90°, which correspond to two potential wells. Thus, the times for the 30° and 90° substeps are

$$t_{\text{mech30}^0} = t_{\text{fluct30}^0} + t_{\text{rotat30}^0} = T/P_{30^0} + \frac{\pi}{6}\xi/\left(\tau_{\text{drive}} - \tau_{\text{load}}\right) \tag{59a}$$

and

$$t_{\text{mech90}^0} = t_{\text{fluct90}^0} + t_{\text{rotat90}^0} = T/P_{90^0} + \frac{\pi}{2}\xi/\left(\tau_{\text{drive}} - \tau_{\text{load}}\right). \tag{59b}$$

Table 1 The parameter values of the motor system

l(nm)	d(nm)	D(nm)	h(nm)	G(N/m^2)	k(pN nm/rad)
7.5	1.25	2.75	5	5×10^7	225
ρ (kg/m^3)	k_T (M^{-1} s^{-1})	k_D (M^{-1} s^{-1})	k_P (M^{-1} s^{-1})	k_{-D} (M^{-1} s^{-1})	k_{-P} (M^{-1} s^{-1})
1000	1.8×10^7	5×10^5	2×10^4	6×10^2	2×10^3

The nonlinear vibration of the γ subunit decides the lowest vibration frequency ω_1 and the root-mean-square error $\left(\sigma_\theta = \sqrt{E\left[\theta_{\text{non}}^2(0,t)\right]}\right)$ of the γ subunit wave. Thus, it has an important effect on the rotation rate of the F_1 motor.

6 Results and discussion

The above equations are utilized for the analysis of the free vibration of the γ subunit. The parameter values of the motor system are given in Table 1. Figures 2, 3, 4, and 5 show changes of the first three vibration frequencies along with system parameters. Tables 2, 3, 4, and 5 give changes of the difference between the nonlinear and linear vibration frequencies along with system parameters. From these results we can conclude:

1. The vibration frequencies of the γ subunit grow with increasing nonlinear parameter ε. This is because the nonlinear stiffness of the γ subunit is larger than the linear stiffness.

As the chemical torque τ_{drive} (written as τ at below) on the γ subunit grows, the natural frequencies of the linear vibration do not change, but the nonlinear free vibration frequencies grow. For larger nonlinear parameter ε, the nonlinear free vibration frequencies grow more obviously with with an increase in the chemical torque.

As the chemical torque τ on the γ subunit grows, the relative errors between the nonlinear and linear free vibration frequencies increase. This is because the nonlinearity of the γ subunit increases with the chemical torque τ. As the order number of the mode

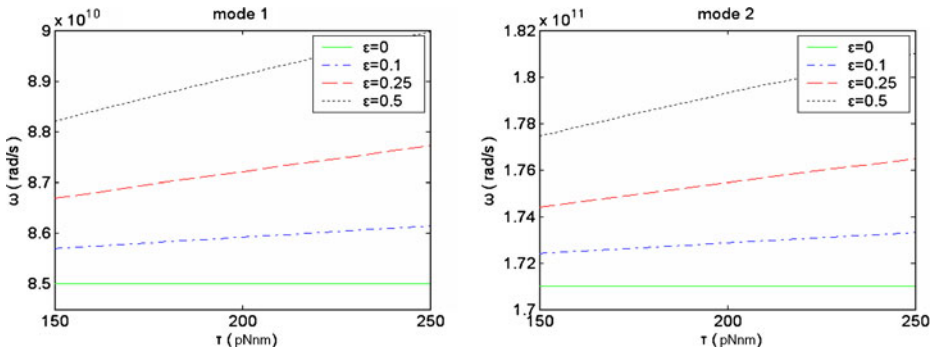

Fig. 2 Changes of the nonlinear vibration frequency along with chemical torque τ_{drive}. **a** mode 1 **b** mode 2

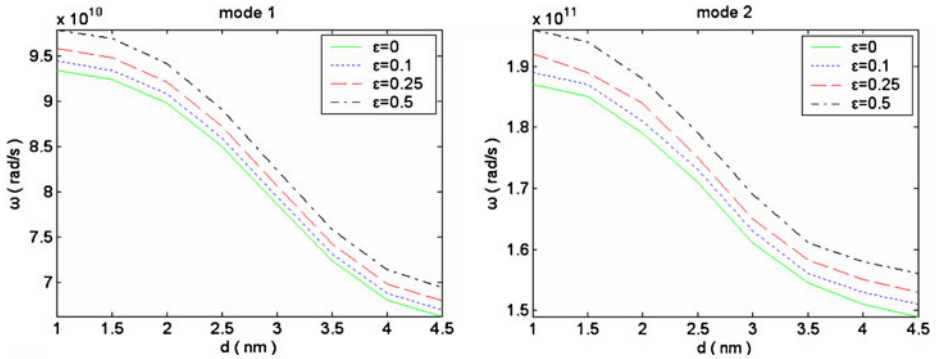

(a) (b)

Fig. 3 Changes of the nonlinear vibration frequency as a function of the γ shaft diameter d. **a** mode 1 **b** mode 2

increases, the effects of the chemical torque τ on the nonlinear free vibration frequencies become small.

For mode 1 and $\varepsilon = 0.25$, the relative errors between the nonlinear and linear free vibration frequencies are 0.9% at $\tau = 25$ pNnm, 1.1% at $\tau = 33$ pNnm, and 1.3% at $\tau = 41$ pNnm. For mode 1 and $\varepsilon = 0.5$, the relative errors between them are 3.7% at $\tau = 25$ pNnm, 4.6% at $\tau = 33$ pNnm, and 5.5% at $\tau = 41$ pNnm.

Hence, the effects of the chemical torque on the nonlinear free vibration frequencies are relatively obvious and cannot be neglected for relatively large nonlinear parameter ε.

2. As the diameter d of the γ subunit grows, the linear and nonlinear free vibration frequencies drop. As the diameter d grows, the relative errors between the nonlinear and linear free vibration frequencies drop for mode 1 and $\varepsilon = 0.25$ or 0.5 (here, the system nonlinearity is relatively strong). This shows that the effect of the diameter d on the nonlinearity of the system drops gradually. For mode 1 and $\varepsilon = 0.1$ or higher order modes (here, the system nonlinearity is relatively weak), the relative errors between the

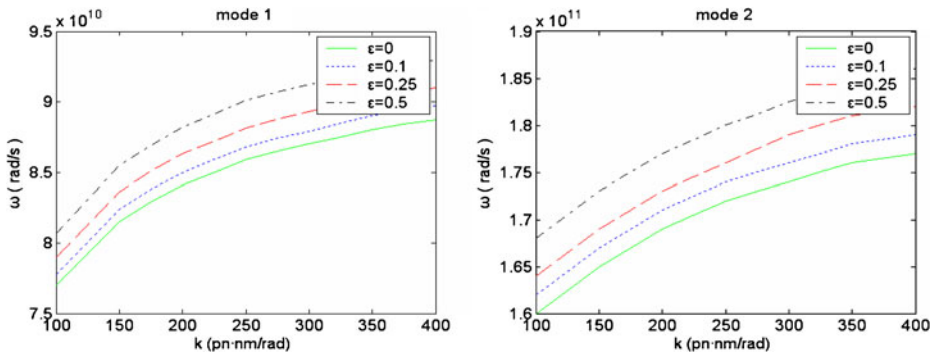

(a) (b)

Fig. 4 Changes of the nonlinear vibration frequency along with stiffness k of the potential well. **a** mode 1 **b** mode 2

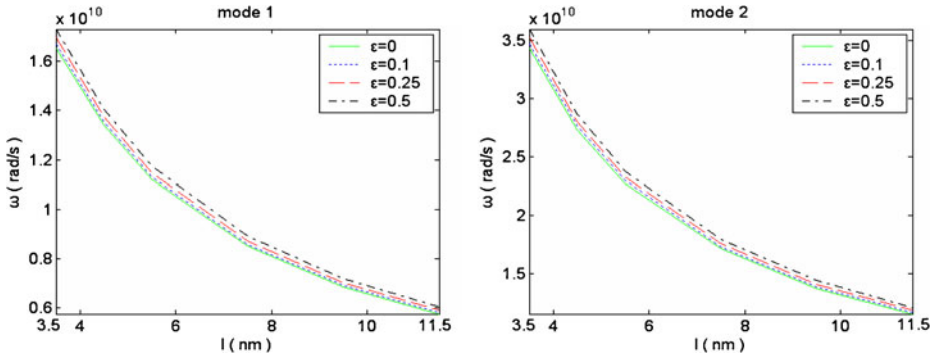

Fig. 5 Changes of the nonlinear vibration frequency along with length l of the γ shaft. **a** mode 1 **b** mode 2

nonlinear and linear free vibration frequencies first grows, reaches a maximum value, and then drops with increasing diameter d.

3. As the stiffness k of the potential well grows, the linear and nonlinear free vibration frequencies grow. As the stiffness k grows, the relative errors between the nonlinear and linear free vibration frequencies change. This shows that the stiffness k has an effect on the nonlinearity of the system as well. As the stiffness k change, the relative errors between the nonlinear and linear free vibration frequencies reach relatively large values at some stiffness k which corresponds to relatively large system nonlinearity.
4. As the length l of the γ subunit grows, the linear and nonlinear free vibration frequencies drop, and the relative errors between the nonlinear and linear free vibration frequencies decrease. This is because the nonlinearity of the γ subunit decreases with the length l.

Changes of the mechanical step time for the γ subunit rotation along with the nonlinear parameter ε are given in Table 6 (here, $\tau_{\text{drive}} = 45$ pN nm and $\tau_{\text{load}} = 0$). Table 7 gives changes of the relative error of the mechanical step time between the nonlinear and linear systems. These results show:

1. When the stiffness nonlinearity of the γ subunit is considered, the mechanical step time for the γ subunit rotation decreases. As the nonlinear parameter ε grows, the mechanical step time for the γ subunit rotation drops further. It should be noted that the nonlinearity has no effect on the jumping time from one well to another. The nonlinearity has an effect only on the oscillation time of the γ subunit within the potential well.

Table 2 The difference between the nonlinear and linear frequencies for various torques τ(pNnm)

τ(pNnm)		25	29	33	37	41
$\Delta\omega_1$	$\varepsilon = 0.1$	0.74×10^9	0.82×10^9	0.92×10^9	1.04×10^9	1.13×10^9
	$\varepsilon = 0.25$	1.71×10^9	2.00×10^9	2.19×10^9	2.49×10^9	2.68×10^9
	$\varepsilon = 0.5$	3.22×10^9	3.71×10^9	4.08×10^9	4.60×10^9	4.96×10^9
$\Delta\omega_2$	$\varepsilon = 0.1$	1.80×10^9	2.00×10^9	2.30×10^9	2.50×10^9	2.80×10^9
	$\varepsilon = 0.25$	3.30×10^9	4.20×10^9	4.90×10^9	5.40×10^9	5.80×10^9
	$\varepsilon = 0.5$	6.60×10^9	7.80×10^9	8.70×10^9	9.70×10^9	1.05×10^{10}

Table 3 The difference between the nonlinear and linear frequencies for various diameters d

d (nm)		1.5	2	2.5	3	3.5
$\Delta\omega_1$	$\varepsilon = 0.1$	0.97×10^9	1.05×10^9	0.92×10^9	0.88×10^9	0.84×10^9
	$\varepsilon = 0.25$	2.38×10^9	2.32×10^9	2.19×10^9	2.11×10^9	1.94×10^9
	$\varepsilon = 0.5$	4.46×10^9	4.40×10^9	4.08×10^9	3.82×10^9	3.49×10^9
$\Delta\omega_2$	$\varepsilon = 0.1$	1.90×10^9	2.00×10^9	2.30×10^9	1.90×10^9	1.30×10^9
	$\varepsilon = 0.25$	5.30×10^9	5.20×10^9	4.90×10^9	3.50×10^9	3.90×10^9
	$\varepsilon = 0.5$	8.80×10^9	8.90×10^9	8.70×10^9	7.60×10^9	7.00×10^9

Table 4 The difference between the nonlinear and linear frequencies for various values of the stiffness k

k(pNnm/rad)		175	200	225	250	275
$\Delta\omega_1$	$\varepsilon = 0.1$	0.91×10^9	1.41×10^9	0.92×10^9	0.90×10^9	0.95×10^9
	$\varepsilon = 0.25$	2.21×10^9	2.23×10^9	2.19×10^9	2.15×10^9	2.32×10^9
	$\varepsilon = 0.5$	4.00×10^9	4.10×10^9	4.08×10^9	4.21×10^9	4.24×10^9
$\Delta\omega_2$	$\varepsilon = 0.1$	1.60×10^9	2.40×10^9	2.30×10^9	2.50×10^9	1.40×10^9
	$\varepsilon = 0.25$	3.90×10^9	4.50×10^9	4.90×10^9	4.40×10^9	4.40×10^9
	$\varepsilon = 0.5$	7.90×10^9	8.10×10^9	8.70×10^9	8.70×10^{10}	8.10×10^9

Table 5 The difference between the nonlinear and linear frequencies for various values of l

l(nm)		3.5	5.5	7.5	9.5	11.5
$\Delta\omega_1$	$\varepsilon = 0.1$	1.8×10^9	1.1×10^9	9.2×10^8	6.7×10^8	6.1×10^8
	$\varepsilon = 0.25$	4.30×10^9	2.80×10^9	2.19×10^9	1.74×10^9	1.46×10^9
	$\varepsilon = 0.5$	8.00×10^9	5.30×10^9	4.08×10^9	3.29×10^9	2.78×10^9
$\Delta\omega_2$	$\varepsilon = 0.1$	3.7×10^9	2.5×10^9	2.3×10^9	1.4×10^9	0.9×10^9
	$\varepsilon = 0.25$	9.00×10^9	5.90×10^9	4.90×10^9	3.50×10^9	2.60×10^9
	$\varepsilon = 0.5$	1.66×10^{10}	1.10×10^{10}	8.70×10^9	6.60×10^9	6.20×10^9

Table 6 Mechanical step times for nonlinear system

ε	t_{nmech} (ms)	$t_{\text{fluct30°}}$ (ms)	$t_{\text{fluct90°}}$ (ms)	$t_{\text{rotat30°}}$ (ms)	$t_{\text{rota90°}}$ (ms)
0.1	0.133	0.031	0.102	0.023	0.047
0.25	0.121	0.028	0.093	0.023	0.047
0.5	0.117	0.027	0.090	0.023	0.047

Table 7 The error of mechanical step time between nonlinear and linear system

ε	τ_{drive} (pN·nm)	τ_{load} (pN·nm)	t_{mech} (ms)	t_{nmech} (ms)	Error (%)
0.1	45	0	0.26	0.133	48.85
0.25	45	0	0.26	0.121	53.46
0.5	45	0	0.26	0.117	55.00

Table 8 The rotation rates at [T] = 0.01 mM

ε	τ_{drive} (pN·nm)	τ_{load} (pN·nm)	[D] (mM)	[P] (mM)	$t_{1/3}$(ms)	v(rps)
0	45	0	0.3	6	8.120	41.05
0.1	45	0	0.3	6	7.993	41.70
0.25	45	0	0.3	6	7.981	41.77
0.5	45	0	0.3	6	7.977	41.79

Table 9 The rotation rates at [T] = 0.1 mM

ε	τ_{drive} (pN·nm)	τ_{load} (pN·nm)	[D] (mM)	[P] (mM)	$t_{1/3}$(ms)	v(rps)
0	45	0	0.3	6	3.116	107.0
0.1	45	0	0.3	6	2.989	111.5
0.25	45	0	0.3	6	2.977	112.0
0.5	45	0	0.3	6	2.973	112.1

Table 10 The rotation rates at [T] = 1 mM

ε	τ_{drive} (pN·nm)	τ_{load} (pN·nm)	[D] (mM)	[P] (mM)	$t_{1/3}$(ms)	v(rps)
0	45	0	0.3	6	2.620	127.2
0.1	45	0	0.3	6	2.493	133.7
0.25	45	0	0.3	6	2.481	134.4
0.5	45	0	0.3	6	2.477	134.6

Table 11 The rotation rates at τ_{load} = 5 pN nm

ε	τ_{drive} (pN·nm)	[T] (mM)	[D] (mM)	[P] (mM)	$t_{1/3}$(ms)	v(rps)
0	45	1	0.3	6	2.629	126.8
0.1	45	1	0.3	6	2.502	133.2
0.25	45	1	0.3	6	2.490	133.9
0.5	45	1	0.3	6	2.486	134.1

Table 12 The rotation rates at τ_{load} = 20 pN nm

ε	τ_{drive} (pN·nm)	[T] (mM)	[D] (mM)	[P] (mM)	$t_{1/3}$(ms)	v(rps)
0	45	1	0.3	6	3.490	95.5
0.1	45	1	0.3	6	3.363	99.1
0.25	45	1	0.3	6	3.351	99.5
0.5	45	1	0.3	6	3.347	99.6

Table 13 The rotation rates at $\tau_{\text{load}} = 35$ pN·nm

ε	τ_{drive} (pN·nm)	[T] (mM)	[D] (mM)	[P] (mM)	$t_{1/3}$(ms)	v(rps)
0	45	1	0.3	6	10.384	32.10
0.1	45	1	0.3	6	10.257	32.50
0.25	45	1	0.3	6	10.245	32.54
0.5	45	1	0.3	6	10.241	32.55

2. As the nonlinear parameter ε grows, the relative error of the mechanical step time for the γ subunit rotation between the nonlinear and linear systems grow. At $\varepsilon = 0.1$, the relative error reaches 48.85%. Hence, the nonlinearity of the γ subunit should be considered. Of course, the relative error could not be so large under a condition in which the chemical reaction time is considered simultaneously.

The effects of the system parameters on the rotation rate of the γ subunit are investigated (see Tables 8, 9, 10, 11, 12, 13, 14, 15, and 16). The Tables show:

1. As the concentration [T] of the ATP grows, the rotation rate of the γ subunit grows obviously. For different [T], the rotation rate of the γ subunit grows with increasing nonlinear parameter ε.

For low [T] (0.01 mM), the increase of the rotation rate of the γ subunit with the nonlinear parameter ε is slow. At [T] = 0.01 mM, relative to the rotation rate of the linear system, the rotation rate of the nonlinear system increases 1.75% for $\varepsilon = 0.25$, and 1.80% for $\varepsilon = 0.5$. Here, the concentration of ATP is low and the binding time for ATP to the β subunit is long, which is the rate limiting step which determines the rotation rate of the γ subunit. Hence, the effect of the nonlinearity on the rotation rate of the γ subunit is weak and can be neglected for low ATP concentration.

As the concentration [T] of the ATP grows, the effect of the nonlinearity on the rotation rate of the γ subunit increases. At [T] = 0.1 mM, relative to the rotation rate of the linear system, that of the nonlinear system increases 4.67% for $\varepsilon = 0.25$, and 4.77% for $\varepsilon = 0.5$. At [T] = 1 mM, relative to that of the linear system, the rotation rate of the nonlinear system increases 5.66% for $\varepsilon = 0.25$, and 5.82% for $\varepsilon = 0.5$. Here, the concentration of ATP is relatively high and the binding time for ATP to the β subunit is short. The rotation rate of the γ subunit depends on the chemical step time and the fluctuation time of the γ subunit within the potential well. The nonlinearity mainly influences the fluctuation time of the γ subunit within the potential well. Hence, the effect of the nonlinearity on the rotation rate of the γ subunit is relatively obvious and should be considered for relatively high ATP concentration.

Table 14 The rotation rates at $l = 5.5$ nm

ε	τ_{drive} (pN·nm)	τ_{load} (pN·nm)	[T] (mM)	[D] (mM)	[P] (mM)	v(rps)
0	45	0	1	0.3	6	129.5
0.1	45	0	1	0.3	6	129.6
0.25	45	0	1	0.3	6	129.7
0.5	45	0	1	0.3	6	129.8

Table 15 The rotation rates at $l = 7.5$ nm

ε	τ_{drive} (pN·nm)	τ_{load} (pN·nm)	[T] (mM)	[D] (mM)	[P] (mM)	v(rps)
0	45	0	1	0.3	6	127.2
0.1	45	0	1	0.3	6	127.3
0.25	45	0	1	0.3	6	127.5
0.5	45	0	1	0.3	6	127.7

2. As the load torque τ_{load} grows, the rotation rate of the γ subunit drops significantly. For different load torque τ_{load}, the rotation rate of the γ subunit grows with increasing nonlinear parameter ε.

For large τ_{load} (35 pN nm), the increase of the rotation rate of the γ subunit with nonlinear parameter ε is slow. At $\tau_{\text{load}} = 35$ pN·nm, relative to that of the linear system, the rotation rate of the nonlinear system increases 1.37% for $\varepsilon = 0.25$, and 1.40% for $\varepsilon = 0.5$. Here, the load torque is large and the jumping time of the γ subunit from one potential well to another is long, which is the rate limiting step. Hence, the effect of the nonlinearity on the rotation rate of the γ subunit is weak and can be neglected for large load torque.

As the load torque drops, the effect of the nonlinearity on the rotation rate of the γ subunit increases. At $\tau_{\text{load}} = 20$ pN·nm, relative to that of the linear system, the rotation rate of the nonlinear system increases 4.19% for $\varepsilon = 0.25$, and 4.29% for $\varepsilon = 0.5$. At $\tau_{\text{load}} = 5$ pN nm, relative to that of the linear system, the rotation rate of the nonlinear system increases 5.60% for $\varepsilon = 0.25$, and 5.76% for $\varepsilon = 0.5$. Here, the load torque is relatively small and the jumping time of the γ subunit from one potential well to another is short. The rotation rate of the γ subunit depends on the chemical step time, the jumping time of the γ subunit from one potential well to another and the fluctuation time of the γ subunit within potential well. Hence, the effect of the nonlinearity on the rotating rate of the γ subunit is relatively substantial and should be considered for relatively small load torque.

3. As the length l of the γ subunit grows, the rotation rate of the γ subunit drops. For different length l, the rotation rate of the γ subunit grows with increasing nonlinear parameter ε.

For different length l (5.5, 7.5, and 9.5 nm), the increase of the rotation rate of the γ subunit with nonlinear parameter ε is slow. At $l = 5.5$ nm, relative to that of the linear system, the rotation rate of the nonlinear system increases 0.15% for $\varepsilon = 0.25$, and 0.23% for $\varepsilon = 0.5$.

As the length l grows, the effect of the nonlinearity on the rotation rate of the γ subunit increases slightly. At $l = 7.5$ nm, relative to that of the linear system, the rotating rate of the nonlinear system increases 0.24% for $\varepsilon = 0.25$, and 0.39% for $\varepsilon = 0.5$. At $l = 9.5$ nm, the rotating rate of the nonlinear system increases 0.24% for $\varepsilon = 0.25$, and 0.40% for $\varepsilon = 0.5$.

Table 16 The rotation rates at $l = 5.5$ nm

ε	τ_{drive} (pN·nm)	τ_{load} (pN·nm)	[T] (mM)	[D] (mM)	[P] (mM)	v(rps)
0	45	0	1	0.3	6	125.1
0.1	45	0	1	0.3	6	125.2
0.25	45	0	1	0.3	6	125.4
0.5	45	0	1	0.3	6	125.6

Hence, the nonlinear effect of the length l changes on the rotation rate of the γ subunit is small and can be neglected for the different lengths.

In a word, the rotation rate of the γ subunit depends on the chemical step time and the fluctuation time of the γ subunit within the potential well. The nonlinearity mainly influences the fluctuation time of the γ subunit within the potential well. Hence, the effect of the nonlinearity on the rotation rate of the γ subunit is relatively obvious and should be considered for relatively high ATP concentration because the chemical step time is short at high ATP concentration and the effects of the fluctuation time of the γ subunit within potential well on its rotation rate are quite clear.

7 Conclusions

In this paper, a nonlinear chemo-mechanical coupled dynamic model of the F_1 motor is proposed. Nonlinear vibration frequencies of the γ shaft and the nonlinear stochastic response of the elastic γ shaft to thermal excitation are investigated. The results show:

1. The stiffness nonlinearity of the γ shaft causes an increase of the vibration frequency for the F_1 motor, which increases the motor's rotation rate.
2. When the concentration of ATP is relatively high, the effects of the stiffness nonlinearity on the rotation rates of the F_1 motor are obvious and should be considered.

References

1. Engelbrecht, S., Junge, W.: ATP synthase: a tentative structural model. FEBS Lett. **414**(3), 485–491 (1997)
2. Boyer, P.D.: The binding change mechanism for ATP synthase – some probabilities and possibilities. Biochim. Biophys. Acta **1140**, 215–250 (1993)
3. Boyer, P.D.: Catalytic site forms and controls in ATP synthase catalysis. Biochim. Biophys. Acta **1458**, 252–262 (2000)
4. Oster, G., Wang, H.Y.: Rotary protein motors. Trends Cell Biol. **13**, 114–121 (2003)
5. Noji, H., Yasuda, R., Kinosita, K.: Direct observation of the rotation of F_1-ATPase. Nature **386**, 299–302 (1997)
6. Sabbert, D., Engelbrecht, S., Junge, W.: Intersubunit rotation in active F_1-ATPase. Nature **381**, 623–625 (1996)
7. Duncan, T.M., Bulygin, V.V., Zhou, Y., Hutcheon, M.L., Cross, R.: Rotation of subunits during catalysis by Escherichia coli F_1-ATPase. Proc. Natl. Acad. Sci. U. S. A. **92**, 10964–10968 (1995)
8. Yasuda, R., Noji, H., Yoshida, M., Kinosita, J.R., Itoh, H.: Resolution of distinct rotational substeps by submillisecond kinetic analysis of F_1-ATPase. Nature **410**(22), 898–904 (2001)
9. Yasuda, R., Noji, H., Kinosita, J.R., Yoshida, M.: F_1-ATPase is a highly efficient molecular motor that rotates with discrete 120° substeps. Cell **93**, 1117–1124 (1998)
10. Gao, Y., Yang, W., Karplus, M.: A structure-based model for the synthesis and hydrolysis of ATP by F_1-ATPase. Cell **123**, 195–205 (2005)
11. Gao, Y., Yang, W., Marcus, R.A., Karplus, M.: A model for the coorperative free energy transduction and kinetics of ATP hydrolysis by F_1-ATPase. Proc. Natl. Acad. Sci. U. S. A. **100**, 11339–11344 (2003)
12. Ming, L.S., Todd, B.D., Sadus, R.J.: Complex cooperativity of ATP hydrolysis in the F_1-ATPase molecular motor. Biochim. Biophys. Acta **1698**, 197–202 (2004)
13. Wang, H.Y., Oster, G.: Energy transduction in the F_1 motor of ATP synthase. Nature **396**, 279–282 (1998)
14. Liu, M.S., Todd, B.D., Sadus, R.J.: Kinetics and chemomechanical properties of the F_1-ATPase molecular motor. J. Chem. Phys. **118**, 9890–9898 (2003)
15. Gaspard, P., Gerritsma, E.: The stochastic chemomechanics of the F_1-ATPase molecular motor. J. Theor. Biol. **247**, 672–686 (2007)
16. Oster, G., Wang, H.Y.: ATP synthase: two motors, two fuels. Structure **7**(4), 67–72 (1999)

17. Panke, O., Cherepanov, D.A., Gumbiowski, K., Engelbrecht, S., Junge, W.: Viscoelastic dynamics of actin filaments coupled to rotary F-ATPase angular torque profile of the enzyme. Biophys. J. **81**, 1220–1233 (2001)
18. Xu, L.: The coupled chemomechanics of the F_1-ATPase molecular motor. Biochim. Biophys. Acta **1777**(12), 1422–1431 (2008)
19. Smith, S., Cui, Y., Bustamante, C.: Overstretching B-DNA: the elastic response of individual double-stranded and single-stranded DNA molecules. Science **271**, 795–799 (1996)
20. Su, T., Purohit, P.K., Bustamante, C.: Mechanics of forced unfolding of proteins. Acta Biomaterialia **5**(6), 1855–1863 (2009)
21. Ikai, A.: Nano-mechanics of proteins with possible applications. Superlattices Microstruct. **31**(1), 43–62 (2002)
22. Fisher, T.E., Oberhauser, A.F., Carrion-Vazquez, M., Marszalek, P.E., Fernandez, J.M.: The study of protein mechanics with the atomic force microscope. Trends Biochem. Sci. **24**(11), 379–384 (1999)
23. Stock, D., Leslie, A.G.W., Walker, J.E.: Molecular architecture of the rotary motor in ATP synthase. Science **286**, 1700–1705 (1999)